ELSEVIER

Journal of Nuclear Materials 273 (1999) 248–256

journal of nuclear materials

www.elsevier.nl/locate/jnucmat

# Amplitude dependent damping study in austenitic stainless steels 316H and 304H. Its relation with the microstructure

G.I. Zelada-Lambri [a], O.A. Lambri [a,b,*], G.H. Rubiolo [b,c]

[a] *Escuela de Ingeniería Eléctrica, Facultad de Ciencias Exactas, Ingeniería y Agrimensura, Universidad Nacional de Rosario, Instituto de Física Rosario (CONICET-UNR), Avda. 27 de febrero 210 bis, 2000 Rosario (SF), Argentina*

[b] *Consejo Nacional de Investigaciones Científicas y Técnicas (CONICET), Argentina*

[c] *Área de Actividad de Materiales, Centro Atómico Constituyentes, Comisión Nacional de Energía Atómica, Avda. Libertador 8250, (1429) Buenos Aires, Argentina*

Received 19 September 1997; accepted 18 February 1999

**Abstract**

The behaviour of the micro-yield stress in AISI 316H and 304H will be related to the shape of the dislocation arrangement that results from different thermomechanical treatments. The physical mechanism which produces the peak in the saturation stress against temperature curve at 623 K, in the fatigue test, will be explained considering the interaction between dislocations and carbon atoms in solid solution. Furthermore, the physical mechanism which controls another peak which also appears in the saturation stress against temperature curve at 823 K will be explained on the basis of an interaction of dislocation with fine precipitates, which contain chromium. This last mechanism allows one to explain the difference in intensity of the peak at 823 K between the 316H and 304H steels. 

## 1. Introduction

The materials employed in nuclear reactors for canning fuel elements or in fusion reactors for the first wall, are subjected to working in very stringent conditions owing to the high temperatures and neutron doses. Good corrosion-resistance and creep and fatigue behaviour favour the austenitic stainless steels as candidate for reactor materials.

Several works have been reported in literature on strain ageing effects in metals [1–7], including austenitic stainless steels [8–11]. In fact, a study of strain ageing effects in 304 and 316 steels was carried out by Armas et al. [11], through low cycle fatigue and transmission electron microscopy (TEM) studies. This work reported the occurrence of dynamic strain aging within the temperature range 523–823 K. A negative strain rate dependence and an increase in the saturation peak stress with temperature were reported within this region. The cells substructures were assumed to be responsible for the enhanced hardness. The appearance of two peaks in the saturation stress against temperature curve at approximately 623 and 823 K was also reported. The first peak was assumed to be controlled by the interaction between the carbon atoms in solid solution and the dislocations. Nevertheless, an explanation could not be given for the mechanism that generates the second peak at 823 K. The authors [11] also reported that the peak height, for the peak at 823 K, in 316H steels was larger than in 304H, but an explanation for this behaviour was not given either.

On the other hand, the damping measurement technique is very sensitive to the microstructural state of the sample and it has been widely applied for studying the defects and their interactions in materials [12,14]. Moreover, the amplitude dependent damping (ADD) measurements reveal very useful information about the interaction mechanism between dislocations and obstacles [13,14]. In fact, several works have been reported on the study of strain aging effects through ADD measurements [15–19].

* Corresponding author. Fax: +54 341 482 1772; e-mail: olambri@fceia.unr.edu.ar

0022-3115/99/$ – see front matter 
PII: S0022-3115(99)00070-7

In this work, TEM, damping measurements and X-ray diffraction studies, were performed in austenitic stainless steels AISI 316H and 304H, under different thermomechanical conditions. A relation between the microstructure and the ADD behaviour was established, in a similar manner as described by Bedford et al. for zirconium [15]. Furthermore, the physical processes that give rise to the appearance of the peaks at 623 and 823 K, in the saturation stress versus temperature curve reported by Armas et al. [11] will be explained.

## 2. Experimental procedure

The samples were austenitic stainless steels AISI 316H and 304H annealed at 1323 K during 1 h and quenched under high vacuum. After annealing, the nominal grain size was about 50 μm. The chemical composition of the employed stainless steels, obtained by means of chemical analysis, was written in Table 1.

Optical metallography of both 316H and 304H steels showed clean grain boundaries, i.e. grains without detectable second phases. The microstructural state of samples after annealing was also checked by means of X-ray diffraction technique. X-ray diffraction studies were performed in transmission mode at room temperature employing the rotate sample device to eliminate directional texture effects. The measurement conditions were 40 KV and 20 mA using the $K_\alpha$ of Cu as incident radiation and monochromator. Previously to X-ray studies the samples were electropolished employing a solution of 90% acetic acid plus 10% perchloric acid at 300 K, for reducing the thickness about 0.3 mm in order to obtain a good diffraction spectrum in transmission mode.

Table 1
Chemical composition in percent for 316H and 304H austenitic stainless steels

| Alloy type | C | Cr | Ni | Mo | Mn |
|---|---|---|---|---|---|
| 316H | 0.068 | 17.79 | 11.20 | 2.55 | 1.85 |
| 304H | 0.045 | 18.78 | 10.23 | 0.32 | 2.00 |

Samples were fatigued in air by means of a screw-driven testing machine, employing fully reversible triangular cycles. The active zone in the sample for fatigue test was a cylinder of 10 mm length and 5 mm radius. Strain was measured on the gauge length of the sample by using extensiometers of high precision and high temperature. Fatigue temperature was measured by a K-type thermocouple spot welded outside of active zone and it was held constant within 1 K, by using a PID temperature controller. The fatigue tests were carried out employing different degree of total strain, $\Delta\varepsilon$, strain rates, $\dot{\varepsilon}$, and temperatures, $T$. The thermomechanical state of the employed samples was summarised in Table 2. The last column indicates the maximum cycle number, $N_{max}$, reached during the fatigue test in the saturation state, before TEM observations and damping measurements. The fatigue test for sample (f)(316/823/0.5/2) was interrupted at 1000 cycles where the saturation state was not even achieved [11,20–22] owing to experimental problems.

Samples for damping measurements were cut from the fatigued cylinders in longitudinal direction employing a low speed cutting machine. The final dimensions were 10 mm length, 2 mm width and 0.2 mm thick.

Damping, $D$, was measured employing a torsion pendulum of inverted type which works at low and high temperatures under high vacuum in the order of $10^{-7}$ Torr in the sample environment [23]. The measurements were carried out at frequencies close to 1 Hz with a run-up and down in temperature at a speed of 0.2 K/min. Recording of the oscillations was made with the usual optical system, including a mirror and a photodiode. The pendulum is driven by an automatic digital data acquisition system based on a PCL 812 card. The

Table 2
Samples thermomechanical state. The numbers sequence in the sample denomination means: steel type, fatigue temperature ($K$); $\Delta\varepsilon$ (%), and $\dot{\varepsilon} \times 10^3$ ($s^{-1}$)

| Sample name | Denomination | Fatigue test/ steel type | Fatigue temp. (K) | $\Delta\varepsilon$ (%) | $\dot{\varepsilon} \times 10^3$ ($s^{-1}$) | $N_{max} \times 10^{-3}$ |
|---|---|---|---|---|---|---|
| a | 316/-/0/0 | No/316H | – | – | – | – |
| b | 316/300/1/2 | Yes/316H | 300 | 1 | 2 | 3 |
| c | 316/523/1/2 | Yes/316H | 523 | 1 | 2 | 3 |
| d | 316/723/1/2 | Yes/316H | 723 | 1 | 2 | 3 |
| e | 316/823/1/2 | Yes/316H | 823 | 1 | 2 | 3 |
| f | 316/823/0.5/2 | Yes/316H | 823 | 0.5 | 2 | 1 |
| g | 316/823/2/2 | Yes/316H | 823 | 2 | 2 | 0.15 |
| h | 316/823/1/0.2 | Yes/316H | 823 | 1 | 0.2 | 3 |
| i | 316/823/1/10 | Yes/316H | 823 | 1 | 10 | 3 |
| j | 316/823/2/10 | Yes/316H | 823 | 2 | 10 | 0.15 |
| k | 304/-/0/0 | No/304H | – | – | – | – |
| l | 304/823/1/2 | Yes/304H | 823 | 1 | 2 | 3 |

damping values were measured in free decay with an error less than 1% [24].

ADD effects were carefully checked as a function of temperature [14,24]. The freely decaying torsional amplitudes $A_n$, $n = 0, 1, 2, \ldots, N$ were measured at constant temperature by means of the data acquisition system. The temperature during the decaying was kept constant with an stability of ±0.2°. On a first step, polynomials were fitted to the data ln $(A_n)$ vs. $n$ representing the decaying oscillations. The damping as a function of amplitude was determined by the first derivative of the polynomial ln $(A_n)$ against $n$. The results were depicted as $D$ against maximum strain on the sample, $\varepsilon_m$. The best fits were obtained with polynomials of degree $\leqslant 3$ [25]. It should be highlighted, that the linearity of the oscillating amplified signal response during the decaying oscillations was accurately checked. The linearity can be assured up to ratios $A_0/A_n = 10\,000$. In fact, this point is crucial for an accurate checking of ADD effects.

Discs for obtaining thin foils were cut, in transverse and longitudinal directions to the specimens axis, from fatigued sample in the saturation state. As a first step the discs thickness was reduced by means of electropolishing employing a solution of 90% acetic acid plus 10% perchloric acid at 300 K. Finally, the thin foils were obtained by means of jet-electropolishing employing an electrolyte of 95% acetic acid plus 5% perchloric acid at 300 K. The observations of thin foils were carried out by means of a TEM operating at 100 kV [20].

## 3. Results and discussion

### 3.1. X-ray diffraction study

The diffraction patterns plotted in Fig. 1 show the diffraction peaks related to the reflection planes (1 1 1) and (2 0 0) of the austenitic phase which appear clearly. Moreover, at $2\theta = 44.72°$ a small peak which has an intensity about 1% of the more intense peak of austenitic phase can be also observed. This peak could be related to the reflection plane (1 1 0) of the δ-ferrite phase. In fact, after the annealing treatment above mentioned only austenite and δ-ferrite should appear; eliminating the martensite phase [26,27]. The quantities of retained δ-ferrite in both 316H and 304H steels, were determined through Rietveld refinement of the X-ray diffraction patterns [28,29]. Those were 3% and 7%, respectively.

### 3.2. Dislocations arrange

Fig. 2 shows the dislocation structures obtained for a sample (h)(316/823/1/0.2). Zones with high and low density of dislocations can be observed. Besides this, non-well-defined cells can be also found. The cells have interiors dislocations and the cells–walls seem to be not

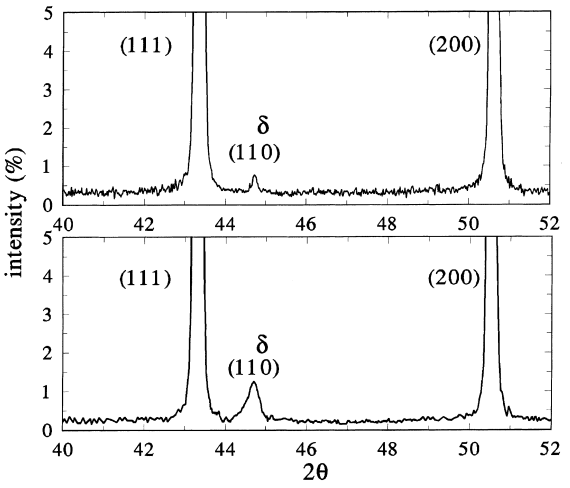


Fig. 1. X-rays diffraction patterns for austenitic stainless steels 316H (upper plot) and 304H (lower plot).

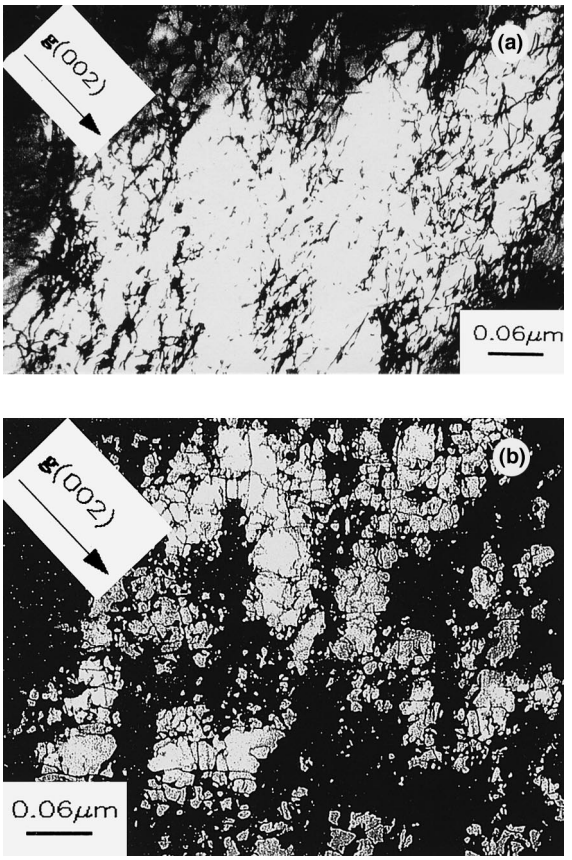


Fig. 2. TEM micrographs for a sample (h)(316/823/1/0.2): (a) Zones with high and low density of dislocations; (b) Non-well-defined cells structure with interior dislocations.


Fig. 3. TEM micrograph for a sample (j)(316/823/2/10) showing a non-well-defined cells structure with interior dislocations.

compacts. A similar dislocation structure was obtained for the kind of samples (c)(316/523/1/2). Fig. 3 shows the dislocation structure obtained for a sample (j)(316/823/2/10) where a non-well-defined cells structure with interiors dislocations can be observed. The cells trend to elongate. Similar characteristics in the dislocation structure were obtained for samples (b)(316/300/1/2), (d)(316/723/1/2) and (i)(316/823/1/10). Fig. 4 shows the dislocations configuration for a sample (e)(316/823/1/2) where well-defined elongated cells and veins structure appear. A dislocation configuration with well-defined elongated cells was also obtained for the kind of samples (l)(304/823/1/2). The dislocation structure obtained for samples (f)(316/823/0.5/2) which is shown in Fig. 5, was of planar array type. Fig. 6 shows the dislocations structure for a sample (g)(316/823/2/2) where can be observed both, an elongated cells array and veins with persistent slip bands (PSB) in [1 1 0] direction. It was also observed that, the compacting degree of the structure and the quantity of grains where the array develops increase with a larger degree of total applied strain, for the set of samples fatigued at 823 K at same strain rate [20]. The results of TEM observations, were summarised in Table 3.

It should be pointed out that, the different kinds of the dislocation structures above reported, were already observed by different authors [11,20–22,30,31].

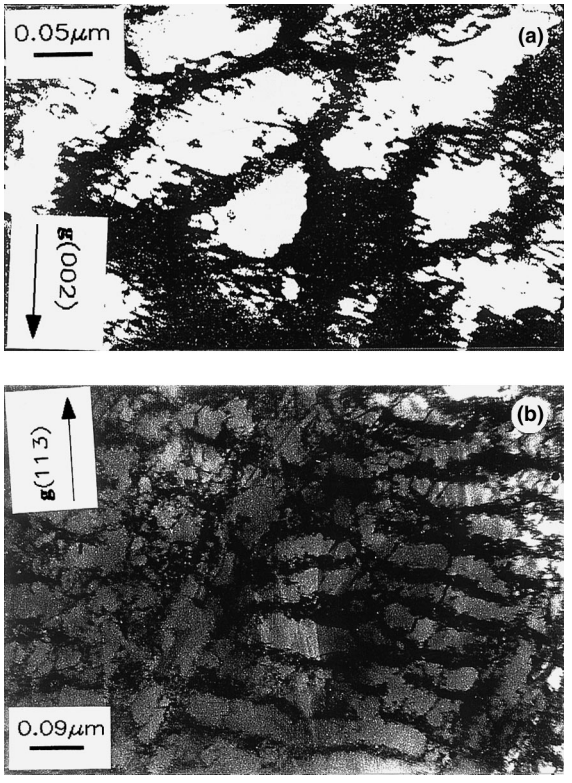


Fig. 4. TEM micrographs for a sample (e)(316/823/1/2): (a) well-defined elongated cells; (b) veins structure.

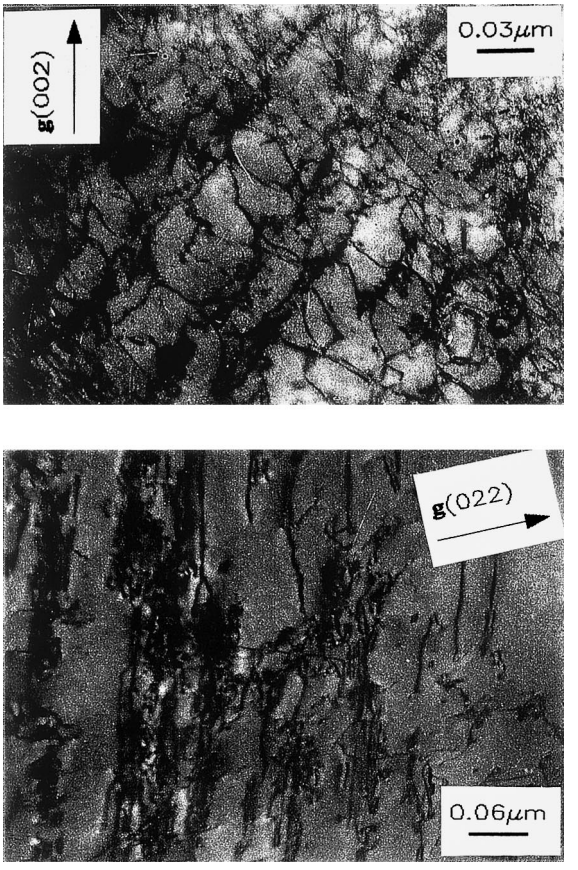


Fig. 5. TEM micrographs for a sample (f)(316/823/0.5/2) showing a planar array type of dislocations.

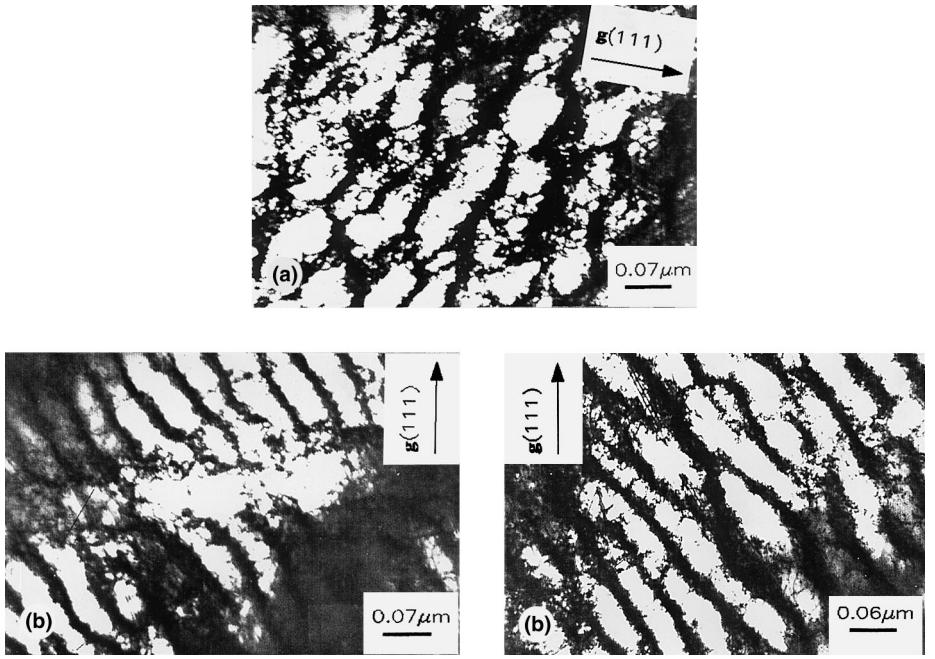


Fig. 6. TEM micrographs for a sample (g)(316/823/2/2): (a) elongated cells array; (b) veins with PSB, in [1 1 0] direction.

### 3.3. Relation between the micro-yield stress and the microstructure

The study of the behaviour of the micro-yield stress under different microstructural conditions can be made through ADD measurements. The critical strain, $\varepsilon_0$, where the ADD effects start can be related to the micro-yield stress. As it was proposed by Granato and Lücke [32], the break-away of dislocation from weak pinning points give rise to the appearance of ADD being $\varepsilon_0$ the transition value between the linear and non-linear damping behaviour [32–34].

Contrary to macroscopic flow stress measurements, in ADD measurements the dislocations are only forced to overcome the weak obstacles, solutes, and not the strong ones. Thus, while the flow stress has contributions from solution hardening and strain hardening, ADD measures only the effects of solutes [16,17]. It should be mentioned that a relation between the macroscopic and microscopic yield stress can be made under determined conditions [35,36], but it will be not discussed in the current work.

Fig. 7 shows the $\varepsilon_0$ behaviour as a function of temperature for all the samples of Table 2. The highest

Table 3
Results of TEM observations for fatigued samples of Table 2

| Sample name | Denomination | Well-defined cells | Elongated cells | Veins | PSB | Planar array | Interiors dislocations | Zones with high and low dislocation densities | Cells trend to elongate | Non-compact cell walls |
|---|---|---|---|---|---|---|---|---|---|---|
| a | 316/-/0/0 | | | | | | | | | |
| b | 316/300/1/2 | | | | | | X | | X | |
| c | 316/523/1/2 | | | | | | X | X | | X |
| d | 316/723/1/2 | | | | | | X | | X | |
| e | 316/823/1/2 | X | X | X | | | | | | |
| f | 316/823/0.5/2 | | | | | X | | | | |
| g | 316/823/2/2 | X | X | X | X | | | | | |
| h | 316/823/1/0.2 | | | | | | X | X | | X |
| i | 316/823/1/10 | | | | | | X | | X | |
| j | 316/823/2/10 | | | | | | X | | X | |
| k | 304/-/0/0 | | | | | | | | | |
| l | 304/823/1/2 | X | X | X | | | | | | |

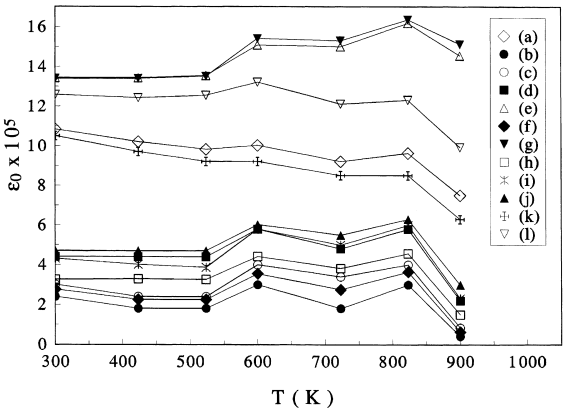


Fig. 7. Critical shear strain for dislocation break-away, $\varepsilon_0$ as a function of temperature for all the samples of Table 2.

levels for break-away of dislocations reported in the figure ($\varepsilon_0 > 12 \times 10^{-5}$), in the whole measured temperature range, occur for samples (e)(316/823/1/2) and (g)(316/823/2/2). Level in $\varepsilon_0$ means the average behaviour of each curve of $\varepsilon_0$ as a function of temperature. Sample (a)(316/-/0/0) shows an intermediate level in $\varepsilon_0$ about $10 \times 10^{-5}$ and the remainder samples, of Table 2, show $\varepsilon_0$ levels smaller than $7 \times 10^{-5}$.

Samples (d)(316/723/1/2), (i)(316/823/1/10) and (j)(316/823/2/10) show an $\varepsilon_0$ behaviour against temperature very similar. Besides this, the $\varepsilon_0$ behaviour for a sample (c)(316/523/1/2) is similar than for a sample (f)(316/823/0.5/2). Sample (h)(316/823/1/0.2) shows an $\varepsilon_0$ level between the samples (c)(316/523/1/2) and (d)(316/723/1/2). Finally, the sample (b)(316/300/1/2) shows the lowest level in $\varepsilon_0$.

An explanation for the different levels in $\varepsilon_0$ curves can be found considering the dislocations array of each sample. In fact, the fatigued samples with a non-well-defined cells structure have shown a low level in $\varepsilon_0$. Meanwhile the samples with a dislocation array of well-defined cells showed higher values in $\varepsilon_0$. As it was pointed out above, the $\varepsilon_0$ behaviour showed in Fig. 7 refers to the interaction process between weak obstacles and dislocations. Therefore, in this work the mobile dislocations lines which produce ADD are the free dislocation lines pinned between strong pinning points, e.g. other dislocations. Consequently, in a structure of non-well-defined cells with interiors dislocations, the free dislocation length (FDL) should be larger than in a structure with well-defined cells being the line stress for the break away of dislocation smaller in the first case [15,34].

It should be pointed out that the occurrence of ADD effects at high values of $\varepsilon_0$ in the annealed samples and fatigued ones with a well-defined cells structure which are free of interiors dislocations, is in agreement with the results of Bedford et al. [12], even if in their work the annealed samples showed amplitude independent behaviour. In fact, they reported that the annealed samples and deformed ones with a well-defined cells structure showed an amplitude independent damping behaviour. However, the authors pointed out that the stress value in damping measurements is well below the yield stress and so the possibility still exists that unpinning of the dislocations may occur at a stress somewhere between the ADD measurements and the yield stress.

In the present work, the oscillating strain was increased up to that ADD effects appeared. As can be seen from Fig. 7, the ADD effects appeared at rather higher strain amplitudes than the maximum strain employed by Bedford et al. ($6 \times 10^{-5}$).

### 3.4. On the peak in the saturation stress vs. temperature curve at 600 K

The behaviour of each $\varepsilon_0$ vs. temperature curve of Fig. 7 will be considered now accurately, i.e. the true behaviour of each curve without consider an associated level (average value) to each one will be study.

As can be seen from Fig. 7 all the $\varepsilon_0$ vs. temperature curves have shown two higher values at 600 and 823 K. Therefore, it could be proposed that at these temperatures, interaction processes between dislocations and solute atoms appear, which increase the $\varepsilon_0$ value. The nature of the interaction process at these temperatures can be checked through the analysis of the damping spectrum as a function of temperature.

Fig. 8(a) shows the damping spectra as a function of temperature for both 316H and 304H steels. The plotted

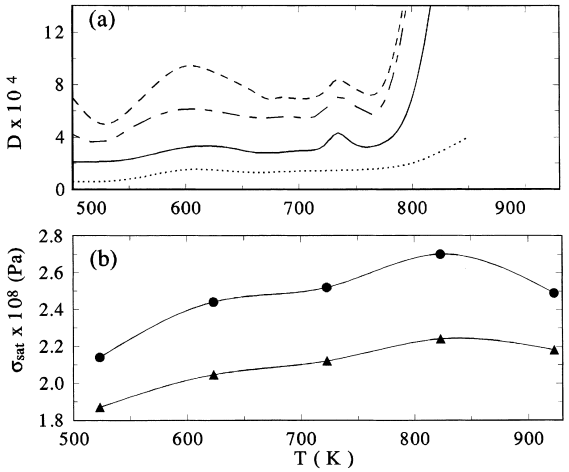


Fig. 8. (a) Damping spectra: full line: sample (a)(316/-/0/0), short dashed line: sample (e)(316/823/1/2)), alt dashed line: sample (e)(316/823/1/2)) during cooling after having reached 1000 K, dotted line: sample (k)(304/-/0/0). (b) Stress saturation as a function of temperature for 316H steel (circles) and for 304H one (triangles).

damping values are the measured ones, i.e. they were not converted to intrinsic damping [14], but it does not obstruct the subsequent analysis.

The appearance of a damping peak at 600 K is well known in cold worked austenitic steels [37–39]. This damping peak could be related to the interaction of dislocation with solute atoms according to the Shoeck model for the cold work peak, but obviously with solutes atoms in a fcc lattice [40]. In fact, as can be seen from figure the peak height increases in the fatigued sample (e)(316/823/1/2), plotted by means of short dashed lines; with respect to the peak height in the annealed one, (a)(316/-/0/0), plotted by means of the full line.

The activation energy of this damping peak, determined from the shift of the peak owing to a shift in frequency was close to the diffusion value of carbon atoms in γ-Fe [39,41]; it was: 113 KJ/mol. Therefore, the damping peak at 600 K in fatigued samples can be related to an interaction mechanism between dislocations and carbon atoms in solid solution. Besides this, the damping peak height in the fatigued samples during cooling after having reached 1000 K decreases (alt dashed line in Fig. 8(a)) owing to the structure recovery and the precipitation of carbon atoms from solid solution at high temperatures [26]. Moreover, the height of the peak in 304 steel is smaller than for 316, owing to a lower carbon content in the 304. These kinds of experimental behaviours are in complete agreement with the physical mechanism above proposed which controls the damping peak at 600 K in fatigued samples.

Fig. 8(a) also shows for samples of 316H alloy a damping peak around 730 K, which is controlled by a physical mechanism unclear yet [42]. However, the appearance of this damping peak does not obstruct the analysis carried out in this work.

A straightforward interpretation leads to propose that the enhances in the micro-yield stress at 600 K is related to the interaction between carbon atoms in solid solution and dislocations.

Fig. 8(b) shows the two peaks in the saturation stress vs. temperature curve at approximately 623 and 823 K, for both 316H and 304H steels, which were already reported in Ref. [11]. As it can be seen from Fig. 8, a good agreement between the peak temperature of the peaks in the $\sigma_{sat}$ curve and the temperature where $\varepsilon_0$ increases (600 K), is achieved. Moreover, the values both in $\varepsilon_0$ and in $\sigma_{sat}$ at 600 K were smaller in the 304H than in the 316H, in agreement with a lower carbon content in 304H than in 316H. Therefore, the assumption made by Armas et al. [11] on the hardening in the $\sigma_{sat}$ curve produced by the interaction between carbon atoms and dislocations at 600 K was verified. Furthermore, a connection between the behaviour of the micro yield stress and the saturation stress against temperature has been found. In fact, an increase in the micro-yield stress leads to an increase in the saturation stress in 316H and 304H.

### *3.5. On the peak in the saturation stress vs. temperature curve at 823 K*

The mean behaviour of $\varepsilon_0$ in both samples of 316H and 304H as a function of temperature, Fig. 7, could indicate the appearance of a precipitation process larger in 316H than in 304H. Although the initial $\varepsilon_0$ levels between samples (a)(316/-/0/0) and (k)(304/-/0/0), and (e)(316/823/1/2) and (l)(304/823/1/2) are similar; it must be highlighted that an increase in temperature leads to a larger decrease in the mean slope of the $\varepsilon_0$ curves in 304H than in 316H ones. In fact, this type of behaviour could be explained on the basis of the appearance of fine precipitates which work like obstacles on the FDL.

The dislocation can overcome the obstacles at a lower stress value in the 304H than in the 316H at the same measuring temperature and microstructural dislocation array owing to a small precipitation degree in the 304H. This smaller quantity of precipitates in 304H than in 316H reduces strongly the value of $\varepsilon_0$ at 823 K in fatigued 304H steel with respect to 316H one, as it can be seen from Fig. 7.

Considering the X-ray patterns of Fig. 1 and Rietveld refinement, it was determined that the 304H steel has a larger quantity of δ-ferrite than 316H one. These quantities of δ-ferrite result in reasonable agreement with the Schaeffler plot [26]. Therefore, the quantity of chromium in solid solution is larger in the 316H steel than in the 304H, leading to a larger precipitation effect in the 316H steel, in agreement with the above exposed.

As it can be seen from Fig. 8(a), the damping background as a function of temperature for 316H samples increases strongly from around 770 K. In contrast, in 304H the damping background also start to increase at approximately the same temperature, but its increasing rate is lower than for 316H. This kind of behaviour could be related to the occurrence of a precipitation process [43,44], which is larger in the 316H steel than in the 304H one in agreement with the difference in the chromium content in solid solution.

On the other hand, observing again the true $\varepsilon_0$ vs. $T$ curves (i.e. without an average value), a peak at 823 K can be seen, Fig. 7. This behaviour in the micro-yield stress for both kind of steels indicates that an interaction process between the dislocations and obstacles appears, around this temperature. This increase was larger in 316H than in 304H. Moreover, the high value in $\varepsilon_0$ vs. temperature curve at 823 K coincides with the peak temperature of the peak in the $\sigma_{sat}$ curve. The peak in $\sigma_{sat}$ is lower in 304H than in 316H, in agreement with the above proposed precipitation process, involving chromium atoms.

The high affinity between the carbon and chromium atoms could form a fine precipitate which would operate as obstacle on the FDL producing the hill in $\varepsilon_0$ and the peak in the $\sigma_{sat}$ curve [26,45,46]. Mulford and Kocks [47] proposed a model based on the dislocation arrested theory originally proposed by Sleeswyk [45,48], for a Ni based alloy which also showed a peak in the saturation stress curve. The difference between the levels in the $\sigma_{sat}$ curve for the 316H and 304H could be related to the difference in the stacking fault value in these steels [22].

## 4. Conclusions

(1) A relation between the dislocation structure and the micro-yield stress was established. The dislocations configurations which resist the highest values of pinning are: Well-defined cells structures without interior dislocations; cells which have walls conformed of complex tangle of dislocations; veins structures.

It should be pointed out that a connection between the micro-yield stress and the saturation stress behaviour could be established. In fact, an increase in the micro-yield stress leads to an increase in the saturation stress in 316H and 304H within the temperature range 500–900 K.

(2) The physical mechanism which controls the peak in the saturation stress vs. temperature curve at around to 623 K was related to the interaction of carbon atoms in solid solution with the dislocations.

(3) The physical mechanism which controls the peak in the saturation stress against temperature curve at around 823 K could be related to an interaction mechanism between dislocations and small precipitates which contain chromium. The peak height in the saturation stress against temperature curve is smaller in the 304H steel than in 316H one, owing to a larger quantity of δ-ferrite in the 304H than in 316H.

## Acknowledgements

This work was partially supported by, the PID-202/98 of the Rosario National University (UNR), the Escuela de Ingeniería Eléctrica, Facultad de Ciencias Exactas, Ingeniería y Agrimensura, UNR and the National Council of Research (CONICET). We wish to express our appreciation to Dr A.B. Labedev for Refs. [35,36] and Dr I.G. Ritchie for Ref. [18].

## References

[1] L.F. Coffin Jr., J. Basic Eng. Trans ASME 87 (1965) 351.
[2] Y. Estrin, L.P. Kubin, in: H.B. Muhlhaus (Ed.), Continuum Models for Materials with Microstructure, Wiley, New York, 1995, p. 395.
[3] I. Bréchet, Y. Estrin, Key Eng. Mater. 97&98 (1994) 235.
[4] J. Schlipf, Acta Metall. Mater. 40 (9) (1992) 2075.
[5] P. Hähner, Mater. Sci. Eng. A 207 (1996) 208.
[6] P. Hähner, Mater. Sci. Eng. A 207 (1996) 216.
[7] S.I. Hong, Mater. Sci. Eng. 79 (1986) 1.
[8] K. Kanazawa, S. Yoshida, in: Proceedings of the International Conference on Creep and Fatigue in Elevated Temperature Applications, Inst. Mech. Engrs. Conf. Publ. 13 (1973) 226.
[9] H. Abdel-Raouf, A. Plumtree, T.H. Topper, Metall. Trans. 5 (1974) 267.
[10] S.P. Hannula, M.A. Korhonen, C.Y. Li, Metall. Trans. A 17A (1986) 1757.
[11] A.F. Armas, O.R. Bettin, I. Alvarez-Armas, G.H. Rubiolo, J. Nucl. Mater. 155–157 (1988) 646.
[12] C. Zener, Elasticity and Anelasticity of Metals, University of Chicago, Chicago, 1956.
[13] A.S. Nowick, B.S. Berry, Anelastic Relaxation in Cristalline Solids, Academic Press, New York, 1972.
[14] B.J. Lazan, Damping of Materials and Members in Structural Mechanics, Pergamon, London, 1968.
[15] A.J. Bedford, P.G. Fuller, D.R. Miller, J. Nucl. Mater. 43 (1972) 164.
[16] R.B. Scharwz, L.L. Funk, Acta Metall. 31 (2) (1983) 299.
[17] R.B. Schwarz, J. Phys. 46 (1985) C10–207.
[18] Z.L. Pan, I.G. Ritchie, N. Bailey, Standard Technical Publication 1169, ASTM (1992) 535.
[19] A. Atrens, J. Nucl. Mater. 55 (1975) 267.
[20] G.I. Zelada, master thesis, Faculty of Science and Engeneering, University of Rosario, Rosario, Argentina, 1990.
[21] G.I. Zelada, I. Alvarez-Armas y, A.F. Armas, in: Proceedings of the Meeting of Argentine Society of Metals, Córdoba, Argentina, 1990, p. 417.
[22] O.R. Bettin, PhD thesis, University of Rosario, Rosario, Argentina, 1989.
[23] O.A. Lambri, Mater. Trans. JIM. 35 (7) (1994) 458.
[24] O.A. Lambri, J. Phys. IV 6 (1996) 313.
[25] B.J. Molinas, O.A. Lambri, M. Weller, J. Alloys Comp. 211&212 (1994) 181.
[26] D.A. Porter, K.E. Easterling, Phase Transformations in Metals and Alloys, Van-Nostrand Reinhold, New York, 1988.
[27] M.F. Ashby, D.R.H. Jones, Engineering Materials, Pergamon, Oxford, 1988.
[28] R.A. Young (Ed.), The Rietvald Method, International Union of Crystallography, Oxford Science, 1993.
[29] J.R. Carbajal, Program FullProf Rietveld Analysis of X-rays and Neutron Powder Diffraction Patterns, 1996.
[30] K.D. Challenger, J. Moteff, ASTM STP 520 (1973) 68.
[31] L. Boulanger, A. Bisson, A.A. Tavassoli, Philos. Mag. A 51 (2) (1985) L5.
[32] A. Granato, K. Lücke, J. Appl. Phys. 27 (1956) 583.
[33] D.H. Niblett, J. Wilks, Adv. Phys. 9 (1960) 33.
[34] J. Friedel, Dislocations, Pergamon, Oxford, 1964.
[35] A.B. Labedev, S.B. Kustov, Phys. Stat. Sol. (a) 116 (1989) 645.
[36] A.B. Labedev, S. Pilecki, Scripta Metall. Mater. 32 (2) (1995) 173.

[37] F. Mezzetti, L. Passari, D. Nobili, in: Fifth International Conference on Internal Friction and Ultrasonic Attenuation in Solids, Aachen, Germany, vol. 75, 1973, p. 436.
[38] S.A. Golovin, K. Belkin, Fiz. Metal. Metallov. 20 (5) (1965) 763.
[39] O.A. Lambri, G.I. Zelada de Lambri, F.M. Saavedra y, A.V. Morón Alcain, Difusao em Materiais, in: J. Philibert, A.C.S. Sabioni y, F. Dyment, Univ. Fed. Ouro Preto, 1996, p. 484.
[40] G. Schoek, Acta Metall. 11 (1963) 617.
[41] T.L. Wu, C.M. Wang, Sci. Sin. 7 (1958) 1029.
[42] O.A. Lambri, G.H. Rubiolo, J.D. Hermida, Mater. Trans. JIM 37 (3) (1996) 218.
[43] G. Schoeck, Phys. Stat. Sol. 32 (1969) 651.
[44] M. Mondino, G. Schoeck, Phys. Stat. Sol. (a) 6 (1971) 665.
[45] O.R. Bettin, private communication.
[46] D.J. Michel, J. Moteff, A.J. Lovell, Acta Metall. 21 (1973) 1269.
[47] R.A. Mulford, U.F. Kocks, Acta Metall. 27 (1979) 69.
[48] A.W. Sleeswyk, Acta Metall. 6 (1958) 598.